Materials and Structures / Matériaux et Constructions
Ref. MS1696 – Resubmitted

Stress-strain characteristic of SFRC using recycled fibres

Authors: H. Tlemat, K. Pilakoutas and K. Neocleous

Centre for Cement and Concrete, Department of Civil & Structural Engineering, The University of Sheffield, UK

Abstract:
This paper presents work from a comprehensive study on the development of a flexural design framework for concrete reinforced with steel fibres that are recovered from used tyres. The experimental flexural behaviour of notched concrete prisms reinforced with these fibres is initially presented. For comparison purposes, prisms reinforced with industrially produced fibres are also considered. An attempt to adopt an existing RILEM design framework to derive appropriate tensile stress-strain blocks is made, but problems are identified with key parameters of the framework. The influence of crack propagation and location of neutral axis depth on the tensile stress distribution is examined. Following an analytical study, it is concluded that the uniaxial stress-strain model, proposed by RILEM overestimates the load-carrying capacity and should be modified by utilising more advanced analytical techniques.

Résumé
Cet article présente une étude sur le développement d'un cadre flexural de conception pour le béton armé à base de fibres d'acier récupérées des pneus utilisés. Le comportement flexural expérimental des prismes en béton entaillés renforcés avec de fibres est initiallement presenté. Aux fins de comparison, des prismes renforcés à base de fibres industriellement produites sont également considérés. Pour déduire les blocs de tension appropriés de contrainte-deformation, une tentative d'adopter un cadre existant de conception de RILEM est effectuée, cependant des problèmes sont identifiés avec les paramètres clé du cadre. L'influence de la propagation de fissure et ainsi que la location de la profondeur d'axe neutre sur la distribution de tension d'effort est examinée. A la suite d'une analyse analytique, on peut conclure que le modèle de contrainte-deformation uniaxial, proposé par RILEM surestime la charge de portance et devrait être modifié en utilisant des techniques analytiques plus élaborées.

1. Introduction

Waste arising from used tyres is currently being managed through the implementation of environmental legislation. In the European Union, the driving force behind the waste management of tyres is the implementation of a number of directives, especially the 1999 Landfill directive [1]. This directive has already stopped the disposal of whole tyres to landfill, and will prohibit the disposal of tyre constituents by 2006. As a result, tyre recycling has become much more popular since it is one of the most environmentally friendly and economically viable ways of managing waste tyres.

Tyre shredding, pyrolysis and cryogenic reduction of tyres are currently the main processes used for the recycling of used tyres. The first process reduces tyres to rubber crumb

and steel fibres. In pyrolysis, tyres are thermally decomposed to their constituents in the absence of air such as oil, gases (hydrogen, methane and other hydrocarbons), carbon, and steel wires. In the cryogenic process the tyre is fractured after being frozen to a suitable temperature.

Research at the University of Sheffield [2, 3, 4, **5**] demonstrated that steel fibres recycled from used tyres (RSF) can be effectively used to reinforce concrete. In addition, it was indicated that the mechanical behaviour of concrete reinforced with tyre-recycled steel fibres (RSFRC) is comparable to that of conventional steel fibre reinforced concrete (SFRC). Therefore, it can be presumed that the design models developed to evaluate the flexural resistance of conventional SFRC are also applicable for RSFRC.

An attempt to use the RILEM design model [6, 7, 8] in FEA simulation for the derivation of flexural behaviour of RSFRC was not successful due to the following reasons. The RILEM model considers almost constant tensile stress in the fracture zone, which is clearly not the case for all fibres, since failure is mainly through pull-out and not yield.

The value used for the load at the limit of proportionality F_u directly affects the determination of the design parameters such as the stress at the limit of proportionality, f_{fct}, and the equivalent flexural strengths, f_{eq2} and f_{eq3}. The authors found that the RILEM procedure for determining F_u [6] does not give consistent results. A Brite-Euram project on SFRC developed an iterative procedure for determining F_u, where a reasonable estimate of the initial slope (between 0.1 and 0.4 of the peak load) is necessary [9]. This project demonstrated that the iterative technique leads to more uniform results, but attempts by the authors to use the procedure did not lead to consistent results. It is noted that the final RILEM recommendation for the σ-ε model uses residual flexural tensile strengths and, hence, the model is independent of F_u.

Finally, two fixed values are considered for the neutral axis depth for the determination of post-cracking flexural tensile strengths (σ_1 and σ_2) after cracking, independent of the amount and type of fibre reinforcement.

This paper describes an experimental study, carried out on RSFRC and SFRC prisms to investigate the above issues. The effect of crack propagation and location of neutral-axis depth on the tensile stress distribution are examined.

The study was carried out on notched prisms by utilising the RILEM bending test [6]. It is noted that a four-point load arrangement was used instead of three-point load. The use of four-point load arrangement created a region of constant moment and, hence, minimised the overestimation of bending resistance, caused at the point of load application by the load-spreading effect [10].

The first part of this paper presents the type of fibres used in this study, and describes the tests performed on prismatic specimens. The second part of the paper examines the effect of fibre type and content on the flexural behaviour of RSFRC and attempts to evaluate appropriate stress-strain relationships by considering the RILEM design model [7, 8].

2. Experimental Examination

2.1 Methodology

2.1.1 Types of fibres and mixes

Two types of RSF were considered: a) pyrolysed and b) shredded. Steel fibres obtained from virgin tyre cord and two types of industrially produced steel fibres were also examined.

The pyrolysed steel fibres (PRSF) were obtained by cutting recycled steel tyre-cord to 50 mm pieces. The cord was obtained from the microwave-induced pyrolysis of whole tyres [11]. The recycled cord was undamaged, since the tyres were decomposed at relatively low temperatures (about 350° C). However, it is noted that the cord was not entirely clean, as it contained a layer of carbon on its surface. In addition, the steel fibre diameter depends exclusively on the type of cord used in the tyre. The typical fibres shown in Fig. 1a were obtained from super-single tyres. The fibres comprised 12 wires of 0.23 mm diameter, twisted together into a core strand of 0.85 mm diameter, and surrounded with another 15 twisted wires. On the cord surface there is a single twisted wire with a twist pitch of 5.33 mm (Fig. 1b). The fibre overall external diameter is 1.55 mm with effective diameter 1.16 mm and a tensile strength in excess of 1250 MPa. In general, the PRSF were not consistent in diameter (ranging 0.8 to 1.55 mm) and shape (Fig. 1a).

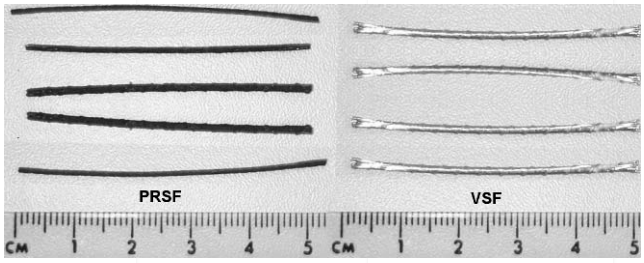

Figure 1a Pyrolysed and virgin steel fibres

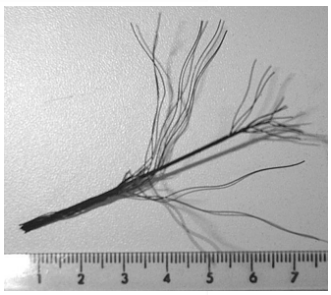

Figure 1b Construction of one pyrolysed fibre

The virgin steel fibres (VSF) were obtained by cutting virgin steel tyre-cord to 50 mm pieces. The VSF fibres were free from any contaminates and had a consistent diameter of 1.55 mm. Their surface and tensile strength were similar to those of PRSF fibres (Fig 1a).

The shredded RSF (SRSF) were obtained from the third stage of mechanical shredding of discarded tyres and, hence, they were inconsistent in diameter and shape (Fig. 2). The SRSF were sieved to avoid using fibres containing rubber crumb on their surface and to remove the larger pieces of steel. In general, the sieved SRSF were more consistent in size and shape and had an average diameter of

0.23 mm, a length averaging over 20 mm and a tensile strength of around 2000 MPa.

Two types of industrially produced steel fibres (ISF) were used and both had a hooked end as illustrated in Fig. 3. The fibres with a flattened end, here called ISF-1, had a length of 50 mm, a nominal diameter of 1mm, and a tensile strength of 1050 MPa. The ISF-2 fibres were made of cold drawn wires, 50 mm long, 1.05 mm thick, and a tensile strength of 1000 MPa (Fig. 3). The geometry and tensile strength of each fibre type are summarised in Table 1.

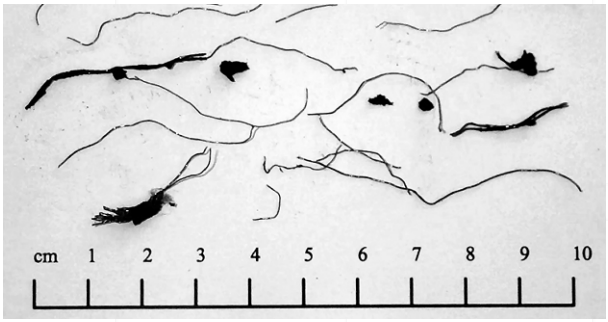

Figure 2 Un-sieved shredded steel fibres

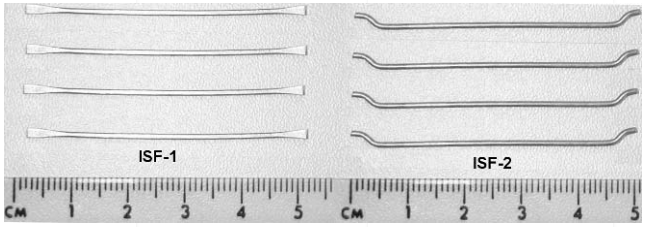

Figure 3 Types of industrially produced steel fibres

Table 1. Summary of geometry and tensile strength for each type of fibre

Fibre type	Length (l)	Diameter (d)	Tensile strength
	[mm]	[mm]	N/mm^2
SRSF	20[a]	0.23[a]	~ 2000
PRSF	50	0.80 – 1.55	>1250
VSF	50	1.55	>1250
ISF-1	50	1.00[b]	1050
ISF-2	50	1.05	1000

[a] average, [b] nominal

Six groups of prisms were cast in the study (see Table 2). In these groups, all sets comprised of three specimens. Group one comprised one set of plain concrete prisms, which were used as control specimens. Group two included three sets of prisms containing SRSF for three fibre ratios (0.5%, 1% and 2% by weight). Groups three and four included three sets of prisms reinforced with PRSF and VSF, respectively, having fibre ratios of 1.5%, 3% and 6% by mass. Groups five and six each comprised of one set of prisms reinforced with high fibre ratio (6% by mass) of ISF-1 and ISF-2, respectively.

Table 2. Material information for each type of prism

Groups: Type of Prism	Fibre ratio	Aspect ratio d/l	SP[3]	Sand	Aggregates		Slump
					10 mm	20mm	
	[%][1]	[-]	[%][2]	[kg/ m^3]	[kg/ m^3]	[kg/ m^3]	[mm]
Plain	0.0	-	0.1	865	345	690	200
SRSF	0.5	≤87	0.2	860	1035	0	160
	1.0	≤87	0.4	855	1035	0	150
	2.0	≤87	0.75	744	1035	0	55
PRSF	1.5	≈32	0.2	851	345	690	200
	3.0	≈32	0.4	837	345	690	150
	6.0	≈32	0.75	807	345	690	140
VSF	1.5	32	0.2	853	345	690	160
	3.0	32	0.4	841	345	690	90
	6.0	32	0.75	815	345	690	70
ISF-1	6.0	50	0.75	815	345	690	150
ISF-2	6.0	48	0.75	815	345	690	150

[1] % by mass, [2] % by cement mass, [3] Superplasticizer

A mix design (SPFA 40/30) with a cement content of 236 kg/m^3 and a water to cement ratio of 0.66 was used for all types of prisms. The coarse and fine aggregate used in this work was fluvial dragged gravel. For practical mixes, the maximum size of coarse aggregate is recommended not to be larger than 2/3 of the length of the steel fibre and should not exceed 1/5 of the minimum size of the specimen [12]. Hence, the aggregates used for plain and SRSF specimens had a maximum size of 10 mm. Two sizes of coarse aggregates were used for the remaining fibres: a) one with a maximum size of 10 mm, and b) one with a maximum size of 20 mm. To improve workability, 30% (by cement mass) of a special SPFA (superpozzolan fly-ash) and various percentages of superplasticizer (Sulphonated Napthalene-Formaldehyde Condensate) were used. Each mix resulted in a set of three prisms and six cubes.

As expected, Table 2 shows that increasing the fibre ratio reduces the workability as measured by the slump test. To obtain a reasonable workability the superplasticizer was increased when the fibre ratio was increased.

2.1.2 Specimen preparation

The prismatic specimens (150 mm deep, 150 mm wide, and 550 mm long) were cast in timber moulds. The specimens were cast in two layers, and were vibrated in the moulds during casting. A day after casting, the specimens were demoulded and then placed in the mist room until the day of testing. A notch (25 mm high and 5 mm thick) was sawn at mid-span, a day before testing, using rotating diamond blades into the tensile face of each beam (perpendicular to the top casting surface) [4, 5]. The purpose of the notch was to act as a crack inducer. All tests were performed at an age shown in Table 3.

2.1.3 Testing procedure

Results from flexural tests on such concrete prisms are prone to significant experimental errors (due to spurious support displacements, machine stiffness and load rate) and, hence, accurate deflection measurements need to be made

[13]. To avoid these errors and the effect of torsion on the deflection measurements, it was decided to use a yoke (Fig. 4) as specified by the Japanese standard [14]. The rollers were pinned and, hence, free to rotate and to allow the expansion of concrete. The specimens were tested in a 100 kN servo-hydraulic machine under displacement control at a constant rate of 0.2 mm/min [4, 5].

Average mid-span beam deflections were measured on both sides of the beam (δ_1 and δ_2) using two transducers fixed to the yoke (LVDT5) and, hence, any torsional effects (due to the roller arrangement) were cancelled out.

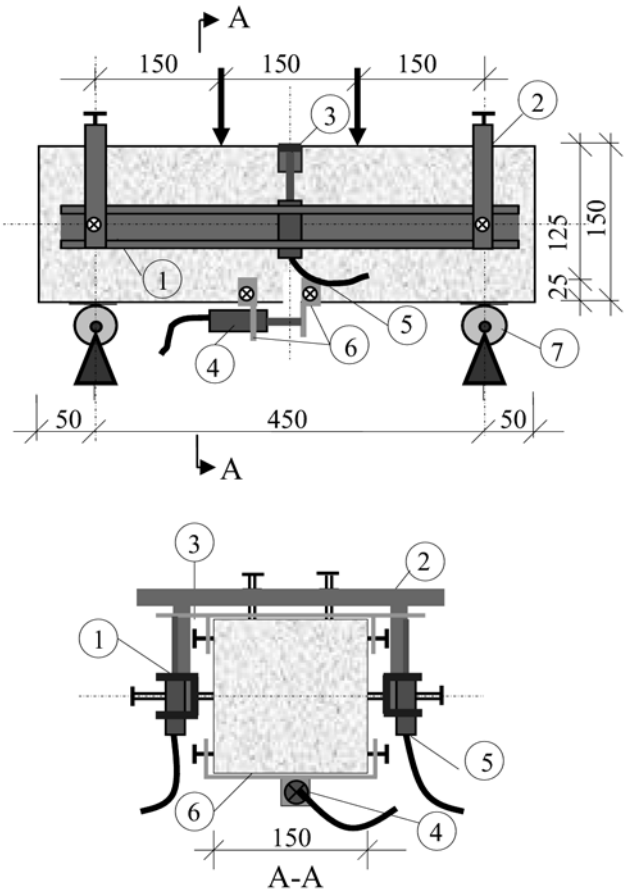

Figure 4 Instrumentation and test set up

One transducer (LVDT4) was mounted across the notch mouth to monitor the crack mouth opening displacement (CMOD). Furthermore, three transducers were used to measure the crack propagation at different height locations, and one transducer was used on the compressive face to measure the compressive strain (Fig. 5).

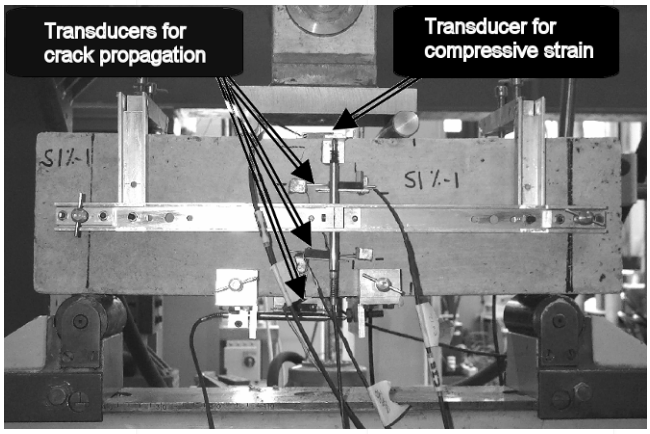

Figure 5 Testing arrangement and instrumentation

2.2 Results

2.2.1 Effect of fibre content and type

2.2.1.1 Compressive strength

For the compressive strength, cubes were placed according to BS 12 [15] with the cast face not in contact with the platens of the testing machine The load was applied at a constant rate of stress within the range of 0.2 to 0.4 (kN / s), and the compressive strength was measured to the nearest 0.5 MPa.

The cylinder compressive strength and the secant modulus needed for the subsequence analysis were calculated according to Eurocode-2 [16] as follows.

$f_{fcm} = 0.85 * f_{cm,}$ [MPa] Equation (1)

$E_{fcm} = 9.5\ f_{fcm}^{2/3}$ [MPa] Equation (2)

Where:

E_{fcm} secant modulus of concrete in compression,
f_{fcm} mean compressive cylinder strength in SFRC,
f_{cm} measured mean compressive cube strength in SFRC.

Table 3 shows the cube compressive strength as the average of six specimens tested on the same day as the corresponding set of prisms. Since different constituents are used in the different mixes, a direct comparison between groups is not easy to make. However, within groups, increased fibre reinforcement appears to increase the compressive strength in all fibres except SFRC. The reduction of strength shown for SFRC 2% may be associated with the reduced workability in that set. Between groups there is only one direct comparison that can be made relating to the sets having 6% fibres. If date of testing is taken into account, no major differences are noted.

2.2.1.2 Flexural strength

Fig. 6 shows the average load-deflection curve for the plain concrete prisms. Point A indicates the load when the first crack is considered to have initiated. On further loading, the plain concrete prism broke suddenly in two halves (Fig. 7). The testing machine was not stiff enough to measure the softening region of plain concrete and no further measurements were recorded.

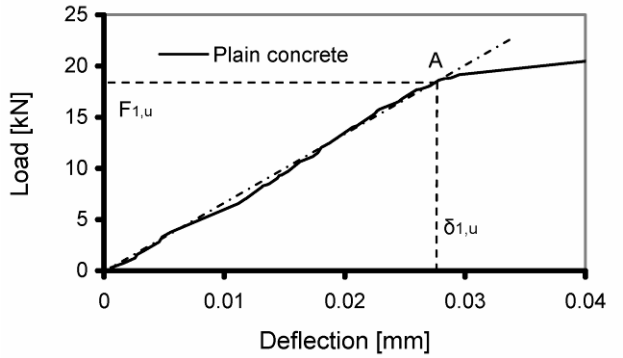

Figure 6 Average load versus mid-span deflection for control beam

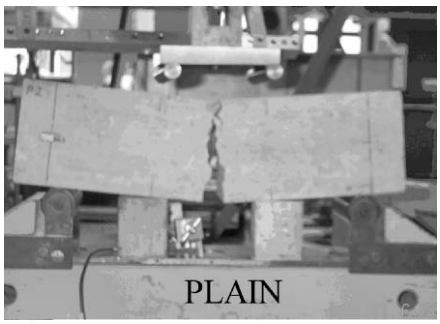

Figure 7 Fracture of plain concrete prism

Fig. 8 shows the average load versus average mid-span deflection for all the SRSF prisms. As expected, the flexural behaviour of the prisms improves as the fibre fraction increases. Fibres act as crack arrestors, giving a substantial increase in toughness, even when fibres debond and are pulling out. In the case of 0.5% fibre ratio, only the toughness was increased. The peak load is 10% lower than of plain concrete, but that can be attributed to the lower compressive strength. However, overall the peak load and the toughness increase with the amount of fibres used.

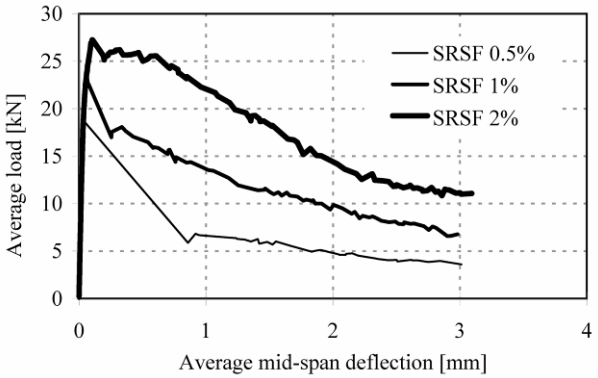

Figure 8 Flexural behaviour of SRSF prisms with different % of fibres

A comparison between PRSF and VSF is shown in Figure 9. The VSF were tested to examine the effect of carbon black on the surface of PRSF. The virgin fibres appear to give higher strength and energy absorption capacity. However, the concrete strength of PRSF (which was tested mush earlier than VSF) is on average 20% less than for VSF, and this on its own may account for this difference. The carbon black on the surface of PRSF appears to increase the workability of the mixes as seen in Table 1. This is surprising since carbon black is a fine powder with a

large surface area. However, the diameter of this powder may be such that it leads to a better packing of the particles of wet concrete. The carbon black may also have an effect on the bond strength of the fibres. However, there is no physical evidence to support that. Since the fibres are mixed by weight and the PRSF fibres have carbon black, this means that less PRSF fibres are used in comparison to VSF. A density examination shows a difference between the two fibres at up to 15%. As less PRSF fibres are used in comparison to VSF, this may explain both the small reduction in energy absorption capacity and the increase in workability.

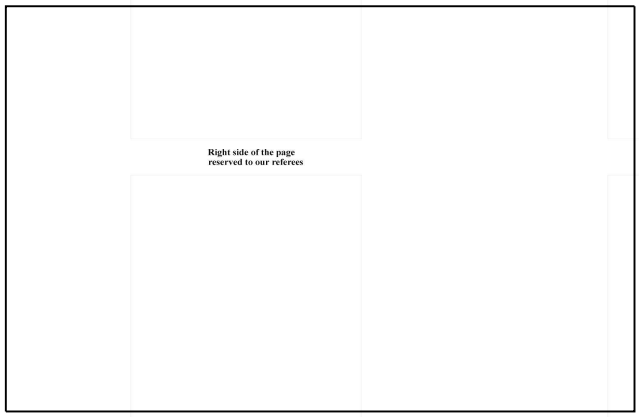

Figure 9 Effects of PRSF and VSF fibre ratios on flexural resistance

Fig. 10 shows that the behaviour of the prism reinforced with 6% ISF-1 and ISF-2 fibres is similar to that of VSF and PRSF prisms. Fibres are pulled out rather than broken during the softening regime. Provided that the fibre bond with concrete is good enough, there should not be much difference between the behaviour of prisms with different fibres, despite the very different nature of the fibres.

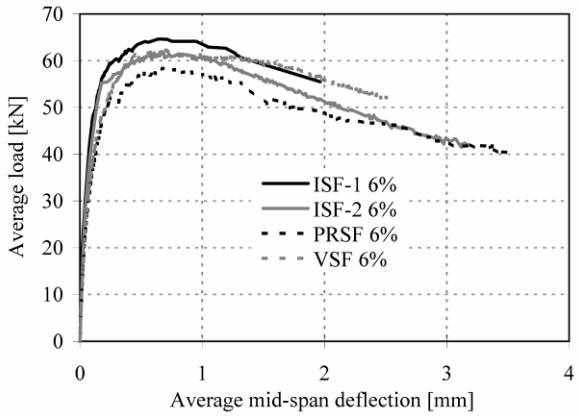

Figure 10 Flexural behaviour of prisms containing 6% ISF, PRSF, and VSF

2.2.2 Pre-crack behaviour

Fig. 11a shows that the initial load-COMD behaviour of prisms containing various ratios of PRSF was linear (region 0-A) until the point of fracture, when the micro cracking phase started (Point A). The region (A-B) is identified as a fracture zone, within which the cracking increases and the stress at the notch tip decreases as the deformation increases.

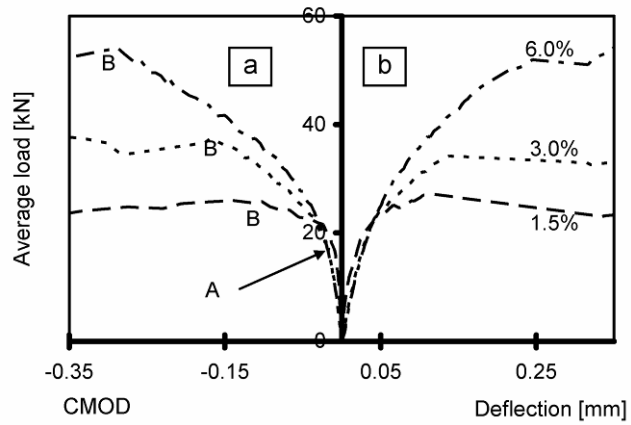

Figure 11 Initial behaviour for prisms containing PRSF

On further deformation, the load also decreases due to complete fibre pull out. The experiments were stopped after the crack exceeded 4 mm. On unloading, the cracks were still visible as shown in Fig. 12.

Figure 12 Fracture of PRSF prism

2.2.3 Flexural strain and crack measurements

To determine the complete strain/crack-width profiles, gauges were used to measure the displacement at fixed points along the depth at mid-span as shown in Fig. 13.

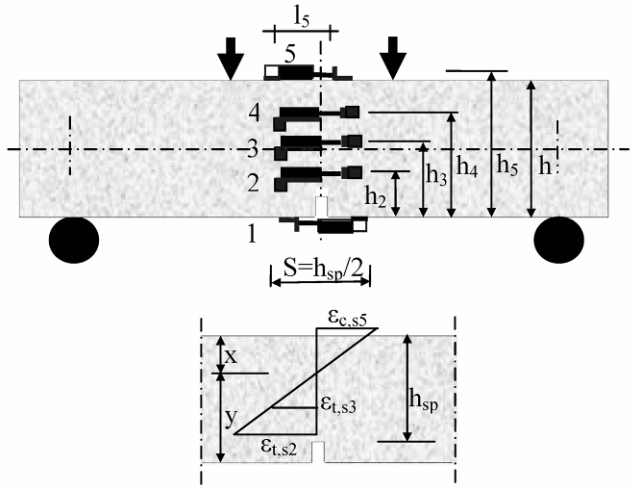

Figure 13 LVDTs Locations and assumed strain distribution

The distance between Gauge 5 and Gauge 2 is equal to h_{sp}. The displacement measured at each gauge can be used to estimate the elastic strain prior to crack initiation and the crack width after crack initiation, as follows.

$u_i = w_{i,el} = l_i \cdot \varepsilon_i$ Prior to crack initiation Equation (3)

Where:

l_i is the length of the gauge
ε_i is the longitudinal strain.

After crack initiation, the displacement may be obtained as the sum of the elastic displacement and the crack opening (equation 4).

$$u_{(i)} = w_{i,el} + w_{i,c} \quad \text{After crack initiation} \qquad \text{Equation (4)}$$

The compressive strain can be determined by dividing the displacement measured by gauge 5 by the length of the transducer l_5 (50mm). The tensile strain prior to crack initiation, at locations h_2, h_3 and h_4 (30, 66 and 117 mm from the bottom surface), respectively, can be determined by dividing the displacement measured by gauges 2, 3 and 4 by a gauge length of 55mm.

Using the cracked hinge model proposed by Ulfkjaer *et al.* [17] and adopted for fibre reinforced concrete by Olesen [18], the tensile strain can be obtained by equation 5.

$$\varepsilon_{t,i} = \frac{\sigma_{i,\max}}{E} + \frac{w_{i.c}}{s} \qquad \text{Equation (5)}$$

Where:

$\sigma_{i,\,max}$ maximum stress at first crack,
$w_{i,c}$ deformation measured after crack initiation,
s length of the hinge.

Obviously, the determination of the length of the hinge is critical in the calculation of strain. Ulfkjaer *et al.* [17] applied the hinge model to a three-point bending beam and obtained a value of s equal to $h_{sp}/2$. This was based on simulated elasto-plastic analysis and comparison with experiments. This result was also confirmed by Olesen [18].

Fig. 14 shows the load versus mid-span deflection and strain at locations 2, 3, 4 and 5 versus mid-span deflection. It can be seen that the compressive strain $\varepsilon_{c0,s5}$ and the tensile strain $\varepsilon_{t0,s2}$ prior to crack initiation (at a deflection corresponding to point A) are more or less equal. The first crack at gauges 2, 3 and 4 was initiated at a load $P_{0,s2}$, $P_{0,s3}$ and $P_{0;s4}$ of 21.4, 28.5 and 32.0 kN, respectively. After crack initiation, the tensile strains $\varepsilon_{c1,s2}$; $\varepsilon_{c1,s3}$; and $\varepsilon_{c1,s4}$ at peak loads (at a deflection corresponding to point B) were 1.31, 0.84 and 0.03 ‰, respectively.

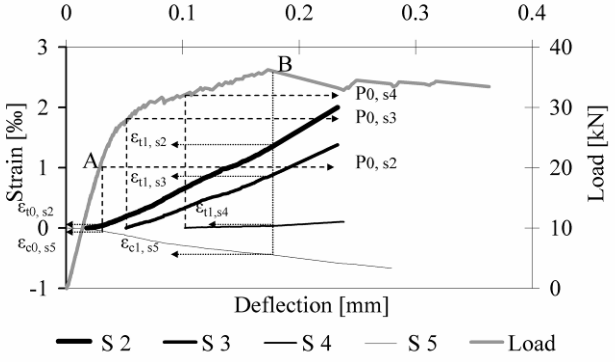

Figure 14 Strain measurements for VSF 1.5%

2.2.4 Position of neutral axis depth

The position of the normalised neutral axis ($y = 1\text{-}x/h_{sp}$) shown in Fig. 15 for a prism reinforced with 1.5% VSF fibres, was calculated using the assumption plane sections

remain plane (Bernoulli). The calculated value of y varied between 0.61 and 0.82 at first micro crack and peak-load, respectively. The maximum depth of the neural axis was 0.95h at a deflection of 3.2 mm. For prisms with higher fibres ratio (3% and 6%), less values were registered, as shown in Fig. 15 for the loads at first-crack, peak and at 3mm deflection. Similar results were reported by Schnuetgen and Dam [19]. It is clear, that the simple approach taken by the RILEM model [7, 8] that the value of y is independent of the fibre volume is not right.

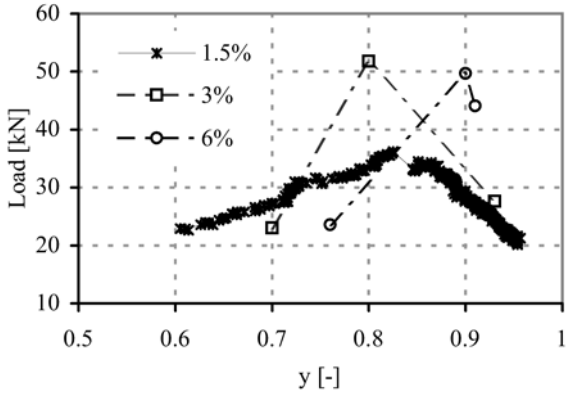

Figure 15 Variation of neutral axis depth for VSF prisms

Using the strain values determined at peak load (Point B, Fig. 14) and the corresponding neutral axis position, the strain profile over the prism's depth can be determined as illustrated in Fig. 16.

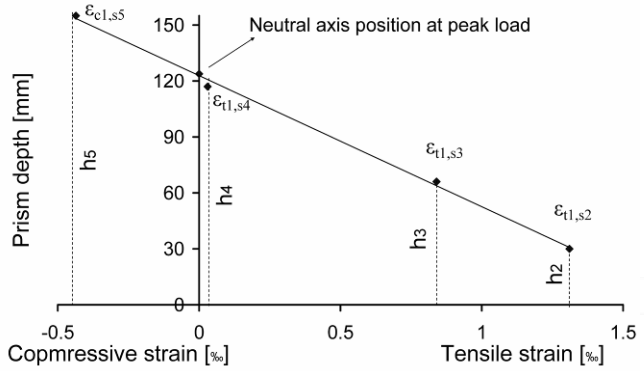

Figure 16 Strain profile over the prism depth

It can be seen that the method to determine the strains and neutral axis position was accurate. This vindicates the choice of hinge length of hsp/2 and can be used as a building block for the development of design models.

2.2.5 Parameters for the determination of stress-strain relationship

To predict the stress-strain curve recommended by RILEM TC 162-TDF [7], the parameters associated with the bending test of the same standard [5] were studied. The limit of proportionality f_{fct} and the equivalent tensile strengths f_{eq1} and f_{eq3} were determined from the load-deflection curve for four-point load tests at several specific deflection values (δ_u, δ_2 and δ_3) as shown in Fig. 17. These values were determined according to DVB [20], from where they were adopted by RILEM.

F_u is the highest value of the load when deflection δ_u does not exceed 0.05 mm. The moment at mid span for the four point test arrangement corresponding to F_u is as follows:

$$M_u = \frac{F_u}{2} * \frac{L}{3} \quad \text{(Nmm)} \quad \text{Equation (6)}$$

Where:

L Support span (mm).

Assuming a linear stress distribution, the limit of proportionality $f_{fct,u}$ can be calculated by equation 7.

$$f_{fct,u} = \frac{F_u * L}{b * h_{sp}^2} \quad \text{(N/mm}^2\text{)} \quad \text{Equation (7)}$$

Where:

b width of the specimen (mm),

h_{sp} distance between the notch tip and the top of the cross section (mm).

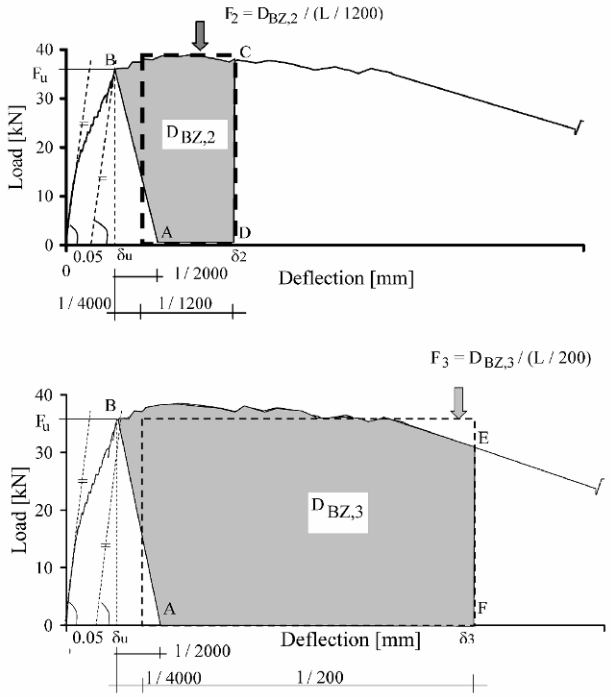

Figure 17 Determination of F_u and equivalent tensile strength.

The energy absorption capacities $D_{BZ,2}$ and $D_{BZ,3}$ are equal to areas ABCD and ABEF under the load-deflection curve up to deflection δ_2 and δ_3, respectively. The mean force recorded in the areas $D_{BZ,2}$ and $D_{BZ,3}$ can be calculated as follows.

$$F_2 = \frac{D_{BZ,2}}{L/1200} \quad \text{(N)} \quad \text{Equation (8)}$$

$$F_3 = \frac{D_{BZ,3}}{L/200} \quad \text{(N)} \quad \text{Equation (9)}$$

The moment at mid span of the corresponding to F_2 and F_3 are determined by equations 10 and 11, respectively.

$$M_2 = \frac{F_2}{2} * \frac{L}{3} = \frac{D_{BZ,2}}{L/1200} * \frac{L}{6} \quad \text{(Nmm)} \quad \text{Equation (10)}$$

$$M_3 = \frac{F_3}{2} * \frac{L}{3} = \frac{D_{BZ,3}}{L/200} * \frac{L}{6} \quad \text{(Nmm)} \quad \text{Equation (11)}$$

The equivalent flexural tensile strength $f_{eq,2}$ and $f_{eq,3}$ can be determined by means of the following expressions.

$$f_{eq,2} = \frac{M_2}{bh_{sp}^2/6} = \frac{F_2 L}{bh_{sp}^2} \quad (\text{N/mm}^2) \text{ Equation (12)}$$

$$f_{eq,3} = \frac{M_3}{bh_{sp}^2/6} = \frac{F_3 L}{bh_{sp}^2} \quad (\text{N/mm}^2) \text{ Equation (13)}$$

In addition, the residual flexural tensile strengths $f_{R,1}$ and $f_{R,4}$, provided by RILEM as a final recommendation [8], were calculated from the load-CMOD curve at CMOD equal to 0.5 mm and 3.5 mm, respectively as shown in Fig. 18.

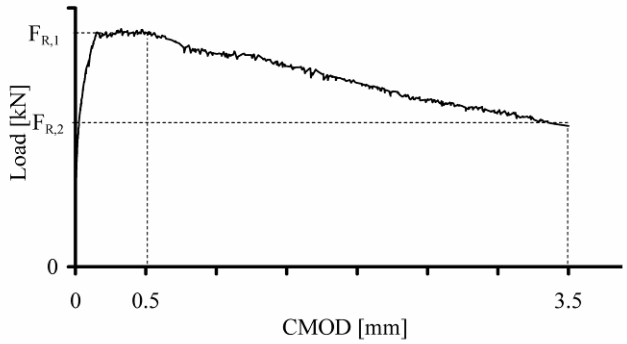

Figure 18 Determination of F_u and residual tensile strengths

$$f_{R,i} = \frac{F_{R,i} L}{bh_{sp}^2} \quad (\text{N/mm}^2) \quad \text{Equation (14)}$$

It should be noted that the CMOD at the bottom surface is calculated using $CMOD_1$ measured at a distance ξ (5 mm) below the prism using the following relationship [21].

$$CMOD = CMOD_1 \frac{h}{h+\xi} \quad (\text{mm}) \quad \text{Equation (15)}$$

$f_{eq,2}$ or $f_{R,1}$ is used in the verification of the serviceability limit states, while $f_{eq,3}$ or $f_{R,4}$ is taken into account at the ultimate limit state. These design parameters were determined for all tested specimens and are tabulated in Table 3.

Table 3 Averaged test results

Groups: Type of Prism	Fibre ratio	f_{cm}	*Age*	F_u	P_{peak}	COV_{Pp} [1]	δ_u	$f_{fct,u}$	$f_{eq,2}$	$f_{eq,3}$	$f_{R,1}$	$f_{R,4}$
	[%]	[MPa]	[Day]	[kN]	[kN]	[%]	[mm]	[MPa]	[MPa]	[MPa]	[MPa]	[MPa]
Plain	0.0	51.5	101	18.0	18.0	9	0.03	3.45	-	-	-	-
SRSF	0.5	49.5	90	18.5	18.5	22	0.05	4.26	1.4	1.6	1.1	0.8
	1.0	50.0	94	23.1	23.1	5	0.06	5.32	2.0	2.8	3.9	1.7
	2.0	45.0	105	27.1	27.1	6	0.08	6.24	2.4	4.1	6.0	2.5
PRSF	1.5	44.0	112	25.1	27.1	7	0.07	5.78	3.3	4.6	5.4	3.7
	3.0	38.5	113	31.7	34.0	15	0.11	7.30	4.3	6.1	7.8	5.8
	6.0	50.0	115	37.4	58.3	15	0.11	8.62	6.3	11.0	12.6	11.2
VSF	1.5	54.1	163	28.7	28.6	11	0.09	6.61	3.2	5.8	6.6	4.3
	3.0	62.0	162	33.4	40.7	23	0.07	7.7	5.2	7.7	10.2	5.2
	6.0	66.2	161	41.6	61.6	23	0.07	9.6	5.9	12.6	14.1	10.4
ISF-1	6.0	52.9	66	44.8	64.6	14	0.09	10.3	6.6	12.4	14.1	12.7
ISF-2	6.0	63.9	196	46.8	61.3	6	0.12	10.78	5.6	11.8	13.8	11.5

[1] coefficient of variation for P_{peak}

The results shown in Table 3 indicate that the equivalent tensile strengths ($f_{eq,2}$ and $f_{eq,3}$) or the residual strengths ($f_{R,1}$ and $f_{R,4}$) of PRSF are slightly lower than for VSF (due to reasons explained earlier). However, the strength characteristics of prisms reinforced with 6% VSF are similar to those for prisms containing 6% of ISF-1 or ISF-2. This can lead to the conclusion that cleaned PRSF fibres are as good as industrial fibres.

The $f_{eq,2}$ and $f_{R,1}$ values for the prism reinforced with 2% SRSF are comparable to those obtained for prisms reinforced with 1.5% of the other types of fibres. However, this is not true for $f_{eq,3}$ or $f_{R,4}$. This indicates that SRSF can be used in applications where bridging of micro cracks is more important than flexural strength.

3. Discussion on Parameters

The results in Table 3 suggest that the relationship between the equivalent flexural tensile strengths ($f_{eq,2}$ and $f_{eq,3}$) and the residual flexural tensile strengths ($f_{R,1}$ and $f_{R,4}$) differs significantly. The residual flexural tensile strength values ($f_{R,1}$) were higher than the values obtained for the equivalent flexural tensile strength $f_{eq,2}$. This is probably as much to do with the definition of these values and the test method as with the accuracy**.** This difference ranged from 1.6 to 2.5 times. This means that the use of both parameters for design purposes, in a similar way as recommended by RILEM, can lead to different results. This problem is related to the fact that the RILEM method for determining the load at the limit of proportionality F_u and the corresponding δ_u is not consistent. Therefore, the evaluation of $D_{BZ,2}$ is inaccurate. The effect of errors in the determination of the initial slope on $f_{eq,3}$ is minor. Fig. 19 shows the relationship between $f_{eq,2}$ and $f_{eq,3}$, and between $f_{R,1}$ and $f_{R,4}$.

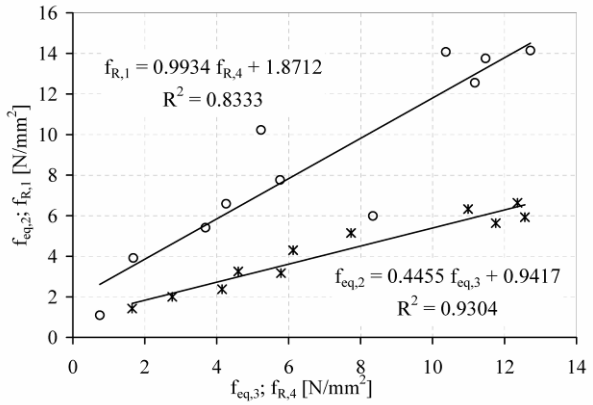

Figure 19 Correlation between equivalent tensile strength and residual tensile strength parameters

Fig. 20, on the other hand, reveals that the residual tensile strength parameter $f_{R,4}$ and equivalent tensile strength $f_{eq,3}$ have similar values but $f_{R,1}$ is greater than $f_{eq,2}$. This indicates that $f_{R,4}$ and $f_{eq,3}$ parameters are insensitive to initial errors and are more appropriate for design purposes.

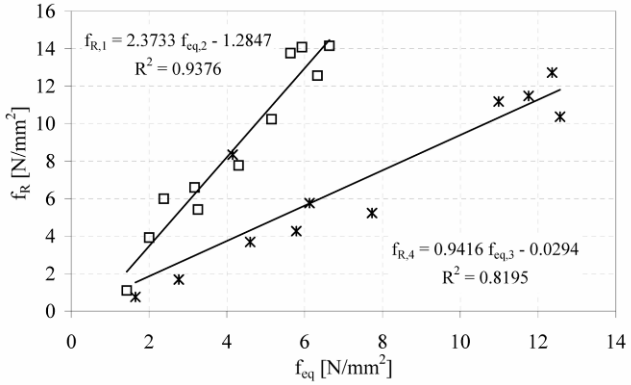

Figure 20 Correlation between f_R and f_{eq}.

4. Analytical investigation of RILEM stress-strain approach

The design recommendation proposed by RILEM appears to overestimate the load-carrying capacity of prisms tested by the Brite-EuRam Project BRPR-CT98-0813 [22]. To investigate the reliability of the RILEM stress-strain model, it is necessary to calculate the load mid-span deflection. For the finite element analysis undertaken by Dupont and Vandewalle of the Brite-EuRam project BRPR-CT98-0813 [22] a relatively simple approximation of the stress-crack width curve was used as input for tensile stiffening. The final stress-strain relationship was then calculated by simply dividing the crack width by the characteristic length, which was assumed to be the length of one finite element. Dupont and Vandewalle [24] assumed the characteristic length to be $0.79h_{sp}$ (h_{sp}, prism effective depth) and the strains were determined by dividing the crack width by two times the assumed characteristic length.

The French recommendation on FRC [25] calculates the strains by dividing the crack width by an assumed characteristic length equal to 2h/3. However, the determination of the value of h is not clearly defined in the recommendation.

The characteristic length (or the width of the fracture zone in a smeared tensile test) is defined by Bazant and Pijaudier-Cabot [26] as the ratio G_F/W_F. The surface fracture energy, G_F, expresses the energy absorbed to create a unit crack area. W_F represents the energy absorbed by a volume of material during a smeared tensile test, where a high number of microcracks are created. Both the surface fracture energy and the volumetric fracture energy are determined from the complete area enclosed by the stress-displacement or stress-strain curves.

In this work, the tested VSF beam with 1.5% fibre ratio was analysed using ABAQUS FE-package [27]. Due to the symmetric boundary, only one half of the prism was analysed. The tension softening effect was modified using the stress-strain curve based on the RILEM design parameters provided in Table 1. Fig. 21 shows the distribution of the principal stresses at peak load. The position of the neutral axis is about $0.8h_{sp}$ at a peak load of 35 kN. This load is higher than that achieved experimentally (Table 3).

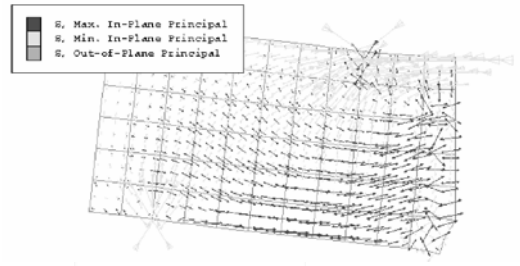

Figure 21 Distribution of the principal stress.

A comparison of the load-deflection curves obtained experimentally and analytically, is shown in Fig. 22. The use of the RILEM stress-strain approach leads to an over estimation of the peak response. In addition, the FE-program was not able to converge after a deflection of 0.12 mm. The overestimation of the load-currying capacity highlights the deficiencies of the RILEM identified earlier and underlines the need for the development of more robust models.

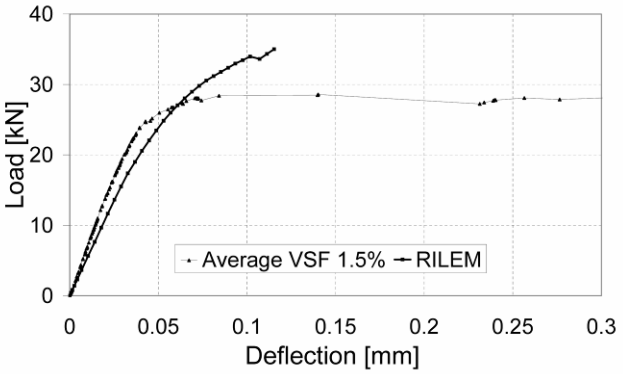

Figure 22 Load-deflection behaviour (result of testing and FEA)

5. Conclusions

The SRSF and PRSF can form a viable alternative to commercially-available steel fibres for use in SFRC. The majority of steel fibre reinforced concrete specimens failed in flexure due to pull-out rather than yielding. The displacement controlled load application lead to stable results throughout the load history.

The equivalent flexural tensile strength for PRSF is slightly lower than that of VSF, due to the lower compressive strength and the black carbon on the PRSF surface. Both ISF prisms and VSF prisms are similar in behaviour. This indicates that cleaned PRSF fibres can be as effective as ISF fibres. Concrete prisms reinforced with 2% SRSF fibre behave similarly to prisms reinforced with 1.5% ISF fibres. SRSF concrete can be used in applications where a high resistance against micro cracking is required.

It is demonstrated here that the neutral axis depth of SFRC migrates with load and should differ for different types and amounts of steel fibres.

The equivalent hinge length of hsp/2 was shown to lead to reasonable results when converting displacement measurements to equivalent strains.

The load at limit of proportionality can not be accurately determined and its use can lead to erroneous estimation of $f_{eq,2}$. The parameter $f_{eq,3}$ can be determined with greater

accuracy and are better parameters for design. The values of the parameters $f_{eq,2}$ and $f_{R,1}$ have great differences contrary to $f_{eq,3}$ and $f_{R,4}$.

A finite element analysis has shown that the stress-strain approach proposed by RILEM overestimates the peak response. A discussion on the characteristic length for determination of strain from crack width shows that there is a diversity of opinions among the researchers and this is also reflected in code equations.

6. Acknowledgements

The authors wish to acknowledge the Marie-Curie EU Community program "Improving Human Research Potential and the Socio-Economic Knowledge Base" under contract number HPMF-CT-2002-01825, the UK Government's Department of Trade and Industry for the partners in Innovation project "Demonstrating steel fibres from waste tyres as reinforcement in concrete" (contract: CI 39/3/684, cc2227) and the University of Sheffield for their financial support.

7. References

1. European Commission, 'Council Directive of 26 April 1999 on the landfill of waste', *Official Journal of the European Communities* **L182** (1999) 1-19.
2. Pilakoutas, K. and Strube R., 'Reuse of tyre fibres in concrete', Proceedings of the International Symposium on Recycling and Reuse of Used Tyres, Dundee, March 2001 (Thomas Telford Ltd, London, 2001) 225-236.
3. Tlemat, H., Pilakoutas, K. and Neocleous, K., 'Pullout behaviour of steel fibres recycled from used tyres', Proceedings of International Symposia on Celebrating Concrete: People and Practice (in Role of Concrete in Sustainable Development), Dundee, Sept. 2003 (Thomas Telford Ltd, London, 2003) 175-184.
4. Tlemat, H., Pilakoutas, K. and Neocleous, K., 'Flexural toughness of SFRC made with fibres extracted from tyres', Proceedings of International Symposium on Advances in Waste Management and Recycling (in Recycling and Reuse of Waste Materials), Dundee, Sept. 2003 (Thomas Telford Ltd, London, 2003) 365-374.
5. Tlemat H., 'Steel fibres from waste tyres to concrete: Testing, modelling and design'. PhD thesis, (Dept. of Civil and Structural Engineering, The University of Sheffield, UK, 2004).
6. RILEM TC 162-TDF, 'Test and design methods for steel fibre reinforced concrete: bending test', *Materials and Structures* **35** (253) (2002) 579-582.
7. RILEM TC 162-TDF, 'Test and design methods for steel fibre reinforced concrete: σ-ε design method', *Materials and Structures* **33** (226) (2000) 75-81.
8. RILEM TC 162-TDF, 'Test and design methods for steel fibre reinforced concrete, σ-ε design method. Final recommendation'. *Materials and Structures* **36** (262) (2003) 560-567.
9. Barr, B. and Lee, M.K., 'Definition of round robin test, preparation of specimens. Execution and evaluation of round robin testing, Final report of Sub-task 2.1 and 2.2', Brite-Euram project BRPR-CT98-0813*:* Test and Design Methods for Steel Fibre Reinforced Concrete, Project funded by the European Community under the

Materials and Structures / Matériaux et Constructions
Industrial & Materials Technologies Programme (Brite-Euram II) (2002).
10. Timoshenko, S.P. and Goodier, J.N., 'Theory of Elasticity', 3rd Edn. (McGraw Hill, New York, 1970).
11. AMAT, 'Advanced molecular agitation technology', (Internet Site: www.amat-ltd.com, 2003).
12. Japan Society of Civil Engineers, 'Recommendation for design and construction of steel fibre reinforced concrete', *Concrete Library of JSCE* **VI** (Article 15) (1994).
13. Copalaratnam, V.S. and Gettu, R., 'On the characterisation of flexural toughness in FRC', *Cement Concrete Composites* **17** (1995) 249-254.
14. Japan Society of Civil Engineers-SF4, 'Methods of tests for flexural strength and flexural toughness of steel fibre reinforced concrete', *Concrete Library of JSCE* (1994) 58-61.
15. British Standards Institution, 'BS 12 - British standard for concrete: method for determination of compressive strength of concrete cubes', (British Standards Institute, London, 1996).
16. European Committee for Standardisation, 'Eurocode 2 - EVV 1992-1-1- Design of concrete structures-Part 1: General rules and rules for buildings', (British Standards Institute, London, 1992).
17. Ulfkjaer, J., Krenk, S. and Brincker, R., 'Analytical model for fictitious crack propagation in concrete beam'. *Journal of. Engineering Mechanics* ASCE **121** (1) (1995) 7-15.
18. Olesen, J. F., 'Fictitious crack propagation in fibre-reinforced concrete beams', *Journal of Engineering Mechanics ASCE* **127** (3) (2001) 272-280.
19. Schnuetgen, B. and Dams, S., ,Stahlfaser im Tunnelbau', Beton-informationen Heft 5-94 (Beton-Verlag, Duesseldor, 1994).
20. DVB, 'Grundlagen zur Bemessung von Industriefussboeden aus Stahlfaserbeton, (Basis for evaluation of steel fibre concrete for use in industrial floors', *Deutschen Beton Vereins* (1995) 258-272.
21. Barr, B. and Lee, M.K., 'Definition of round robin test, preparation of specimens, execution and evaluation of round Robin testing - report of subtasks 2.1 and 2.2', Brite-Euram project BRPR-CT98-0813*:* Test and Design Methods for Steel Fibre Reinforced Concrete, Project funded by the European Community under the Industrial & Materials Technologies Programme (Brite-Euram II) (2002).
22. Hemmy, O., 'Recommendations for finite element analysis of FRC - report of subtask 3.5', Brite-Euram project BRPR-CT98-0813*:* Test and Design Methods for Steel Fibre Reinforced Concrete, Project funded by the European Community under the Industrial & Materials Technologies Programme (Brite-Euram II) (2002).
23. Dupont, D. and Vandewalle, L., 'Recommendations for finite element analysis of FRC – report of subtask 3.5', Brite-Euram project BRPR-CT98-0813*:* Test and Design Methods for Steel Fibre Reinforced Concrete, Project funded by the European Community under the Industrial & Materials Technologies Programme (Brite-Euram II) (2002).

24. Dupont D. and Vandewalle, L., 'A practical proposal to drive a stress-strain relation with residual tensile strengths – annex 5.1.3', Brite-Euram project BRPR-CT98-0813*:* Test and Design Methods for Steel Fibre Reinforced Concrete, Project funded by the European Community under the Industrial & Materials Technologies Programme (Brite-Euram II) (2002).
25. Resplendino, J. and Petitjean, J. `French recommendations for ultra-high performance fibre-reinforced concretes`. Test and Design Methods for Steel Fibre Reinforced Concrete – Background and Experiences- Proceedings of the RILEM TC 162-TDF Workshop. Edited by B. Schnetgen and L. Vandewalle. Germany
26. Bazant, Z. P. and Pijaudier-Cabot, G., 'Measurement of characteristic length of non-local continuum', *Journal of Engineering Mechanics (ASCE)* **115** (4) (1989) 755-767.
27. Hibbitt, Karlsson and Sorensen Inc., 'Abaqus User's Manual', Vol. II, Version 6.1, PP 11.5.1.1-11.5.1.14 (USA, 200).